

The role of electric charge in microdroplets impacting on conducting surfaces

Weiwei Deng and Alessandro Gomez^{a)}

Department of Mechanical Engineering, Yale University, 9 Hillhouse Avenue, New Haven, Connecticut 06520, USA

(Received 19 February 2010; accepted 29 April 2010; published online 24 May 2010)

A rich phenomenology is revealed by temporally resolved image sequences of electrically charged ethanol microdroplets impacting on a conductive surface at temperatures bracketing the liquid boiling point. Notable phenomena include the flattening of the sessile droplets with reduced contact angle, increased evaporation rates for substrate temperatures below the fluid boiling point, and the hindrance of droplet rebound at the Leidenfrost temperature. Scaling considerations are presented to rationalize the observed behavior and to generalize conclusions to a broader droplet size range.

© 2010 American Institute of Physics. [doi:10.1063/1.3431739]

The impact of microdroplets on a solid substrate is of growing interest, with intense research activities on controlled deposition by maskless, bottom-up fabrication techniques for the production of many novel functional structures.^{1–4} Although the dominant deposition method is based on ink-jet printing (IJP), electrospray (ES) techniques⁵ are coming to the fore,^{6,7} as they offer an appealing alternative because of their control on droplet size down to submicrons, a scale much smaller than that achievable by IJP. Therefore ES has the potential to achieve higher spatial resolution in the deposited materials.⁷ Furthermore, increased deposition rates by orders of magnitude through multiplexing ensure that application requirements can be met.^{8,9} The problem is also relevant to desorption ES ionization in which electrosprayed charged droplets are impacted onto a surface to be chemically analyzed.¹⁰ The issue of how the presence of electric charge on the droplets affects the impact process is yet to be addressed. On dielectric surfaces, not surprisingly, the electric charge was shown to increase the maximum spread of droplets.¹¹ For conductive surfaces, on the other hand, one would expect that the charge be promptly neutralized. We will show that for the microdroplets of interest in applications the electric charge may in fact play a significant role in the phenomenology ensuing droplet impact.

The droplet impact dynamics can be classified in terms of the Weber number $We = \rho d v_0^2 / \gamma$ and the Ohnesorge number $Oh = \mu / (\rho \gamma d)^{1/2}$, the first representing the ratio of inertial force to surface tension one, while the second relates the viscous force to inertial and surface tension forces. In their definition, ρ is the liquid mass density, v_0 is the droplet impacting velocity, d is the droplet diameter before impact, γ is the liquid interfacial tension, and μ is the liquid dynamic viscosity.¹² For typical ES droplets impacting a grounded surface, $We \sim O(10)$ and $Oh \sim O(0.1)$, corresponding to a relatively gentle impact with droplet spreading, but without

splashing. The additional parameter that has a significant effect is the surface temperature T_s .

Figure 1 depicts the experimental setup, which consists of three major components: an ES source (a stainless steel needle), an impacting target, and a high-speed camera. The ES source is charged at voltage V_1 , while an extractor electrode nearby is charged at V_2 . The ES is operated in the cone-jet mode, generating quasimonodispersed droplets in the [16–62 μm] diameter range, depending on the flow rate, with typical relative standard deviation smaller than 10%. All tests are performed using ethanol, a liquid with good electro-spraying properties. Its electrical conductivity K is measured at $K = 1.3 \times 10^{-5}$ S/m. In some cases, we use corona discharge to neutralize the droplets and study their impact in the absence of electrostatic interactions. The droplet impact target is a thin, polished stainless steel plate that is electrically grounded and mounted on a cartridge heater. The distance between the extractor and the substrate is fixed, and the impact velocity can be adjusted by varying V_2 , while keeping $V_2 - V_1$ a constant. The impact processes are recorded with a high speed camera (Phantom v7.3, Vision Research, Wayne, NJ).

Figure 2 shows the rich phenomenology captured by time-resolved image sequences of a charged microdroplet impacting on the conducting surface with T_s in the 58–150 °C range, bracketing the liquid boiling point (78 °C). For each sequence, T_s , d , and impact velocity v_0 are reported in the first column. Figure 1(a) is a representation of a typical three-stage sequence:

- (i) Impact (0–20 μs), during which the droplet contacts the substrate and deforms from a sphere to a liquid disk reaching a maximum spread diameter;
- (ii) recoil (20–45 μs), during which surface tension drives the liquid back to a liquid hemispherical cap, which may oscillate several times after the initial recoil;
- (iii) quasisteady evaporation (≥ 45 μs), during which the sessile droplet retains its flattened shape and shrinks gradually until the evaporation is complete at 3.5 ms.

^{a)} Author to whom correspondence should be addressed. Electronic mail: alessandro.gomez@yale.edu. Telephone: 203-432-4384. Fax: 203-432-7654.

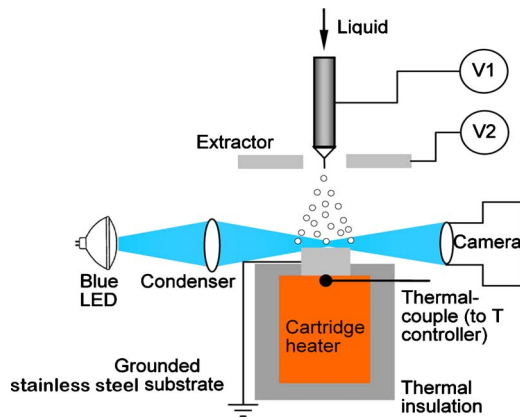


FIG. 1. (Color online) Experimental setup for charged droplet impact.

The impact dynamics at 78 °C [Fig. 2(b)] and 100 °C [Fig. 2(c)] is similar to that at 58 °C, except for larger contact angle, higher recoil amplitude, and shorter evaporation time at higher temperatures. At temperatures corresponding to the well-known Leidenfrost point,¹³ the rebound may or may not be suppressed, depending on the droplet size and impact velocity, as shown for $T_s = 120$ °C [Figs. 2(d)–2(f)], or the droplet is quickly pulled back to the surface, at 150 °C [Fig. 2(g)]. Further details of sequences (a)–(c) and (d)–(g) are discussed below.

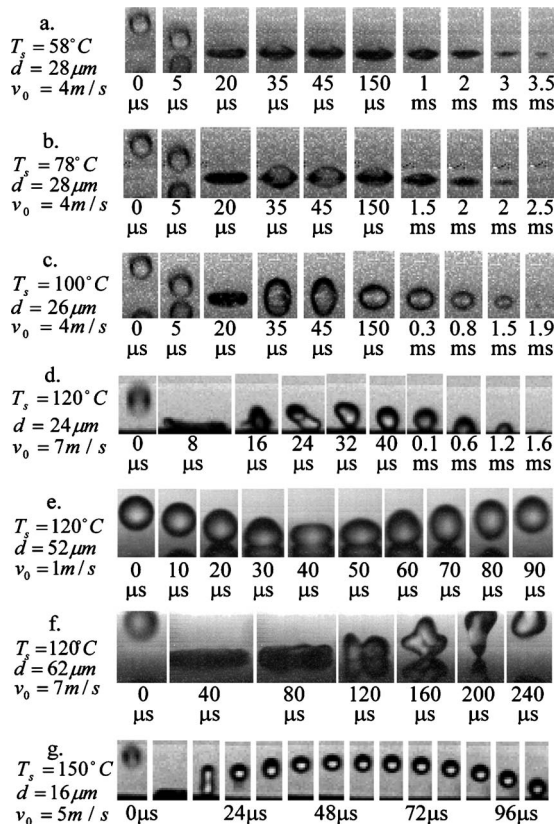
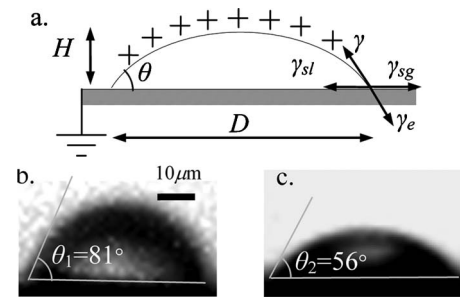


FIG. 2. Temporally resolved image sequences of charged microdroplets impacting on a heated polished stainless steel surface at temperatures ranging from 58 to 150 °C.

FIG. 3. (a) Interfacial stress on a charged liquid spherical cap with height H and base diameter D . (b) Sessile neutral droplet and (c). Charged sessile droplet for $T_s = 78$ °C. The contact angles are derived from $H/D = (1 - \cos \theta)/2 \sin \theta$.

At the lower temperatures [sequences (a)–(c)], the sessile droplet behavior is not qualitatively different from that of neutral microdroplets,^{14–16} but for the role of the image force resulting from the integration of the Maxwell stress, $\tau_e = \epsilon_0 E^2/2$, at the liquid/gas interface, where ϵ_0 is the dielectric permittivity of the medium (air) surrounding the liquid, and E is the electric field at the interface. The latter is related to the surface free charge density σ_e through $E = \sigma_e/\epsilon_0$. The magnitude of the image force can be estimated using a liquid spherical cap model, as shown in Fig. 3(a). When the droplet reaches maximum spread, roughly 1/2 of the initial charge q is lost through the bottom of the droplet contacting the conducting surface. The surface area of the hemispherical cap ($\theta \leq 90^\circ$) is $A_{\text{cap}} = [4/(2 + \cos \theta)]^{1/3} A_0 \sim A_0$, where A_{cap} is the surface area of the spherical cap and A_0 is the surface area of the droplet before impact. Consequently, the surface charge density of the spherical cap is approximately 1/2 of that of the droplet before impact, or $\sigma_e = \sigma_0/2$, and $\tau_e = \tau_0/4$. Implicitly, we assumed negligible evaporation and the remaining charge at the liquid/gas interface to be “frozen” during the very short impact and recoil times, which implies that the charge relaxation time $t_e = \epsilon/K$ is sufficiently long, where ϵ is the dielectric permittivity of the liquid and $\epsilon/\epsilon_0 = 25.3$ for ethanol at room temperature. σ_e is bound by the Rayleigh limit,¹⁷ that is, $\sigma_e \leq (8\gamma\epsilon_0/d)^{1/2}$, requiring that the Maxwell stress does not exceed the interfacial stress, i.e., $\tau_R = 4\gamma/d$. Because the charge level of the ES generated droplets is typically at 50%–80% of the Rayleigh limit,¹⁸ we eventually obtain $\tau_0 \sim \gamma/2d$.

This image force, if the charge is not quickly transferred to the substrate upon impact, is sufficiently large to cause qualitative and quantitative changes in the impact behavior. For the typical values of the experimental conditions, i.e., $\gamma = 0.0224$ N/m and $d = 30$ μm, we obtain $\tau_e \approx 400$ Pa and an image force $F_e \approx \tau_e A_0 \approx 1$ μN, that is 1000-fold the weight of the droplet. Figures 3(b) and 3(c) show an example of the effect of image force on two sessile droplets: a neutral one and a charged one. We notice an obvious change in the contact angle from a value of 81° for the neutral droplet to 56° for the charged one. Application of the Young–Laplace equation to the neutral droplet yields $\gamma_{sg} - \gamma_{sl} = \gamma \cos \theta_1$, where γ_{sg} and γ_{sl} are interfacial tension for solid-gas and solid-liquid interfaces, respectively. For a charged droplet, the electric charge causes an additional tension γ_e along the

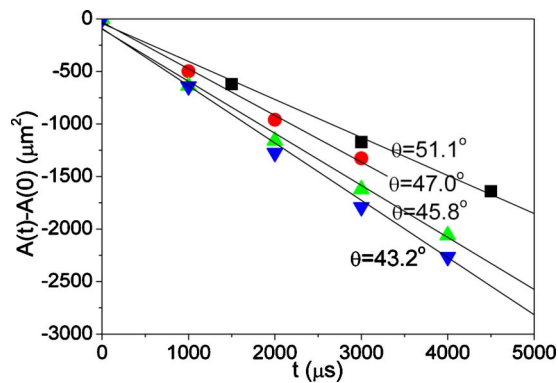


FIG. 4. (Color online) Evaporation rate for different contact angles ($T_s = 58^\circ\text{C}$).

liquid-gas interface that *de facto* weakens the surface tension spheroidizing effect and pulls the liquid toward the grounded surface. The Young–Laplace equation now becomes $\gamma_{sl} - \gamma_{st} = (\gamma - \gamma_e) \cos \theta_2$, where θ_2 is the new contact angle. Combining the two equations yields $\gamma_e = \gamma(1 - \cos \theta_1 / \cos \theta_2)$. On the basis of the measured values of the contact angles, we obtain $\gamma_e = 0.6\gamma$, which yields an estimate of the electric stress $\tau_e \sim \gamma_e / D \sim 0.3\gamma / d$, within a factor of 2 of the liquid spherical cap model.

One significant effect caused by the change in contact angle is on the evaporation rate of a sessile droplet. Smaller contact angles resulting from the electric stress yield larger ratios of surface area to volume, and eventually faster evaporation rate. Figure 4 shows the evaporation of four droplets with apparent contact angle varying from 43.2° to 51.1° as a result of different charge levels on the droplet. The evaporation can be described by $A(t) = A(0) - Ct$, where t is time, $A(t)$ is the surface area of the liquid cap, and C is the evaporation constant for each evaporating liquid cap. In Fig. 4, C is the slope of the fitted lines. As expected, the slope is steeper for smaller contact angles, which is in agreement with the relationship derived in Ref. 19.

When T_s is sufficiently larger than the fluid boiling point, a thin vapor layer forms between the bottom of the droplet and the substrate upon impact. This condition corresponds to the well-known Leidenfrost point. At this point, the contact angle is nearly 180° and a microdroplet generally tends to experience rebound. As the charged microdroplet is subject to a significant image force, a picoliter droplet does not rebound [Fig. 2(d)]. For the same surface temperature, on the other hand, larger droplets (~ 0.1 nl) do experience rebound, as shown in Figs. 2(e) and 2(f). To understand this behavior one has to compare the charge relaxation time, $t_e \sim 16 \mu\text{s}$, for the liquid under examination, to the impact time, given by $t_{\text{im}} = 8d/3v_0$.²⁰ For $t_{\text{im}} > t_e$, charge transport from the droplet to the conducting surface is completed during contact and the image force plays no role in the postimpact developments. This is the case for the larger droplets (~ 0.1 nl) with relatively long contact time, at 50 and 70 μs in Figs. 2(e) and 2(f), respectively. Consequently, both droplets experience rebound, in sharp contrast with the sequence in Fig. 2(d) for the same surface temperature, where the droplet is pinned to the surface. At an even higher temperature, T_s

TABLE I. Scaling of relevant physical processes affecting the impact of a charged droplet on a heated conducting surface. g in the last row is the standard gravity.

Scaling parameter	Femtoliter droplet	Picoliter droplet	Nanoliter droplet
d	2.5 μm	25 μm	250 μm
$V = \pi d^3/6$	8 fl	8 pl	8 nl
$t_{\text{im}} = 8d/3v_0$	1.3 μs	13 μs	133 μs
$t_e = \epsilon/K$	16 μs	16 μs	16 μs
$t_v = h^2/\nu$	0.1 μs	11 μs	1.1 ms
t_v/t_{im}	$O(0.1)$	$O(1)$	$O(10)$
$a_{\text{im}} = \gamma/\rho d^2$	$10^5 g$	$10^3 g$	10 g

$= 150^\circ\text{C}$, the charged microdroplet first rebounds because of the thicker vapor cushion between the droplet and the surface and is quickly attracted back to the surface [Fig. 2(g)]. We can construct the displacement function $y(t)$ by tracking the center of mass displacement of the droplet as a function of time, deriving velocity, acceleration, kinetic energy, and electric potential energy after rebound, and estimating the amount of charge remaining on the droplet. In Fig. 2(g), after impact, the droplet loses 90% of the original kinetic energy, as a result of strong viscous energy dissipation. The estimated amount of charge is 6×10^{-14} C, which is 40% of the Rayleigh limit, confirming that a significant amount of charge remains on the droplet even after the impact. The calculated acceleration is $O(1000g)$ and is consistent with the previous estimate.

Table I summarizes the relevant scaling of competing physical processes for droplets of various sizes. The table lists, in addition to droplet size and volume, impact time, t_{im} , charge relaxation time, t_e , viscous time t_v , the ratio of the latter to the impact time, t_v/t_{im} , and the acceleration a_{im} due to image force, i.e., $a_{\text{im}} = F_e/m = \pi\gamma d/8/(\rho\pi d^3/6) \sim \gamma/\rho d^2$. For a significant amount of charge to remain on the droplet after impact, $t_{\text{im}} < t_e$, which is certainly satisfied for the femtoliter droplet. For the intermediate case of picoliter droplet, we have already shown that the electric charge has a dramatic effect on the contact angle. For nanoliter or larger droplets, on the other hand, t_{im} is much longer, which suggests that charge transport from the droplet to the conducting surface is completed during contact.

The viscous time is defined as $t_v = h^2/\nu$, where ν is the liquid kinematic viscosity. The characteristic length scale is h , the height of the flattened splat,²¹ given by $h = 2d^3/3d_{\text{max}}^2$, where d_{max} is the maximum diameter of splat that can be computed using an energy balance and is typically $2d$, under the present experimental conditions. As shown in Fig. 2(g), viscous damping does appear to dissipate much of the droplet kinetic energy during impact in the case of the small droplets. The characteristic time ratio t_v/t_{im} gauges the relative importance of viscous dissipation to the convection of droplet kinetic energy. The image force is unlikely to play a role if this ratio is much larger than unity. On the other hand, for small values of t_v/t_{im} , the majority of the convected kinetic energy will be dissipated on impact. Under these conditions, the image force is sufficiently strong to bring the droplet back to the substrate.

In summary, temporally resolved sequences of the impact of charged picoliter droplets on a conducting surface for different surface temperatures show that the image force experienced by the droplet plays a significant role on the postimpact history, so long as the droplet charge level before impact is sufficiently high and a significant fraction of the charge remains on the droplet after the initial impact. If the surface temperature is at or below the liquid boiling point, the image force prevents any rebound and leads to enhanced evaporation rate of the flattened, sessile droplet. Above the Leidenfrost point, the image force either prevents the droplet from bouncing off the surface or promptly pulls it back to the surface. Scaling arguments demonstrate that the importance of the image force is not a foregone conclusion and, in fact, does not apply to larger, nanoliter droplets.

The support of the U.S. Army (Grant No. W911NF-05-2-0015) is gratefully acknowledged.

- ¹J. F. Dijkman, P. C. Duineveld, M. J. J. Hack, A. Pierik, J. Rensen, J.-E. Rubingh, I. Schram, and M. M. Vernhout, "Precision ink jet printing of polymer light emitting displays," *J. Mater. Chem.* **17**, 511 (2007).
- ²B. Winther-Jensen and F. C. Krebs, "High-conductivity large-area semi-transparent electrodes for polymer photovoltaics by silk screen printing and vapour-phase deposition," *Sol. Energy Mater. Sol. Cells* **90**, 123 (2006).
- ³B. R. Ringeisen, C. M. Othon, J. A. Barron, D. Young, and B. J. Spargo, "Jet-based methods to print living cells," *Biotechnol. J.* **1**, 930 (2006).
- ⁴P. A. Meléndez, K. M. Kane, C. S. Ashvar, M. Albrecht, and P. A. Smith, "Thermal inkjet application in the preparation of oral dosage forms: Dispensing of prednisolone solutions and polymorphic characterization by solid-state spectroscopic techniques," *J. Pharm. Sci.* **97**, 2619 (2008).
- ⁵M. Cloupeau and B. Prunet-Foch, "Electrostatic spraying of liquids in cone-jet mode," *J. Electrostat.* **22**, 135 (1989).
- ⁶I. W. Lenggoro, H. M. Lee, and K. Okuyama, "Nanoparticle assembly on patterned 'plus/minus' surfaces from electrospray of colloidal dispersion," *J. Colloid Interface Sci.* **303**, 124 (2006).
- ⁷J.-U. Park, M. Hardy, S. J. Kang, K. Barton, K. Adair, D. K. Mukhopadhyay, C. Y. Lee, M. S. Strano, A. G. Alleyne, J. G. Georgiadis, P. M. Ferreira, and J. A. Rogers, "High-resolution electrohydrodynamic jet printing," *Nature Mater.* **6**, 782 (2007).
- ⁸W. Deng, C. M. Waits, B. Morgan, and A. Gomez, "Compact multiplexing of monodisperse electrosprays," *J. Aerosol Sci.* **40**, 907 (2009).
- ⁹W. Deng, J. F. Klemic, X. Li, M. A. Reed, and A. Gomez, "Increase of electrospray throughput using multiplexed microfabricated sources for the scalable generation of monodisperse droplets," *J. Aerosol Sci.* **37**, 696 (2006).
- ¹⁰Z. Takáts, J. M. Wiseman, B. Gologan, and R. G. Cooks, "Mass spectrometry sampling under ambient conditions with desorption electrospray ionization," *Science* **306**, 471 (2004).
- ¹¹S. U. Ryu and S. Y. Lee, "Maximum spreading of electrically charged droplets impacting on dielectric substrates," *Int. J. Multiphase Flow* **35**, 1 (2009).
- ¹²S. Schiaffino and A. A. Sonin, "Molten droplet deposition and solidification at low Weber numbers," *Phys. Fluids* **9**, 3172 (1997).
- ¹³J. D. Bernardin, C. J. Stebbins, and I. Mudawar, "Mapping of impact and heat transfer regimes of water drops impinging on a polished surface," *Int. J. Heat Mass Transfer* **40**, 247 (1997).
- ¹⁴D. B. van Dam and C. Le Clerc, "Experimental study of the impact of an ink-jet printed droplet on a solid substrate," *Phys. Fluids* **16**, 3403 (2004).
- ¹⁵H. Dong, W. W. Carr, and J. F. Morris, "Visualization of drop-on-demand inkjet: Drop formation and deposition," *Rev. Sci. Instrum.* **77**, 085101 (2006).
- ¹⁶T. Lim, S. Han, J. Chung, J. T. Chung, S. Ko, and C. P. Grigoropoulos, "Experimental study on spreading and evaporation of inkjet printed picoliter droplet on a heated substrate," *Int. J. Heat Mass Transfer* **52**, 431 (2009).
- ¹⁷L. Rayleigh, "On the equilibrium of liquid conducting masses charged with electricity," *Philos. Mag.* **14**, 184 (1882).
- ¹⁸K. Tang and A. Gomez, "On the structure of an electrostatic spray of monodisperse droplets," *Phys. Fluids* **6**, 2317 (1994).
- ¹⁹H. Hu and R. G. Larson, "Evaporation of a sessile droplet on a substrate," *J. Phys. Chem. B* **106**, 1334 (2002).
- ²⁰M. Pasandideh-Fard, Y. M. Qiao, S. Chandra, and J. Mostaghimi, "Capillary effects during droplet impact on a solid surface," *Phys. Fluids* **8**, 650 (1996).
- ²¹S. Chandra and C. T. Avedisian, "On the collision of a droplet with a solid surface," *Proc. R. Soc. London, Ser. A* **432**, 13 (1991).